Effect of surface area on electrical properties of NiCo2O4-reduced graphene oxide nanocomposites for supercapacitor electrodes applications

by Cek Turnitin Oi

KeAi
CHINESE ROOTS
GLOBAL IMPACT

Effect of surface area on electrical properties of NiCo$_2$O$_4$-reduced graphene oxide nanocomposites for supercapacitor electrodes applications

Andriono Manalu [a,b], Kerista Tarigan [d], Syahrul Humaidi [a,*], Masno Ginting [c], Istas Pratomo Manalu [d], Ikhwanuddin [e]

[a] Post Graduate Program (Physics), FMIPA, Universitas Sumatera Utara, Jln Bioteknologi No 1, Medan 20155, North Sumatra, Indonesia
[b] Department of Physics Education, Faculty of Teaching Training and Education, Universitas HKBP Nommensen Pematang Siantar, Pematang Siantar 21132, North Sumatra, Indonesia
[c] Physics Research Center, Badan Riset dan Inovasi Nasional (BRIN), South Tangerang, Banten 15314, Indonesia
[d] Department of Computer Engineering, Faculty of Informational Studies, Del Institute of Technology, Toba 22381, Indonesia
[e] Department of Agricultural Products Technology, Faculty of Agriculture, Universitas Islam Sumatera Utara, Medan 20217, North Sumatra, Indonesia

ABSTRACT

Based on the method of electrical charge storage, supercapacitors are divided into two categories, double-layer electrical capacitor (EDLC) and pseudocapacitors. Utilizing three processes—reversible adsorption, redox reactions on metal oxides, and reversible electrochemical—pseudocapacitors are utilized for high power applications involving metal oxide electrodes and the transfer of electric charge based on a reversible faradaic. In the fabrication of supercapacitors, a high specific surface area with a relatively narrow pore size distribution is essential. Therefore, it is required to increase the capacitance of the material. In this work, nickel cobaltite (NiCo$_2$O$_4$) synthesized from nanocomposite NiS·5H$_2$O and Co$_2$SO$_4$·7H$_2$O precursors were mixed with reduced graphene oxide (rGO). Coprecipitation and calcination were used to create the nanocomposites. The produced NiCo$_2$O$_4$/rGO nanocomposite was used as a pseudocapacitive supercapacitor electrode. The results showed that sample code S2 with mass variations of NiO, Co$_3$O$_4$, and rGO at a ratio of 2:3:2 had the best performance. The sample had a hexahedron-shaped surface morphology, an average particle size of about 0.005 m^2, a specific surface area of 12.75 m^2/g, an average pore radius of 9.534 nΩ.m, and a pore volume of 0.06404 cm^3/g. It also performed exceptionally well in terms of electrical conductivity of 6.078 S/m, electrical resistivity of 0.16 nΩ.m, and capacitance of 289.32 F/g.
© 2022 The Authors. Publishing services by Elsevier B.V. on behalf of KeAi Communications Co. Ltd. This is an open access article under the CC BY-NC-ND license (http://creativecommons.org/licenses/by-nc-nd/4.0/).

1. Introduction

As a developing country, Indonesia has a significant need for a variety of resources to advance. This also contributes to the expanding use of electronic components in the energy, transportation, technology, and information technology industries. The increasing use of electronic component materials each year will increase the electricity demand, including electrical energy storage components, causing the development of electrical energy storage component devices to garner a great deal of attention [1]. A supercapacitor is one of the frequently utilized electrical energy storage materials. A supercapacitor or electrochemical capacitor is an electrical double layer that functions as an electrical energy storage device based on charging and discharging at the electrode-dielectric interface [2]. Currently, the supercapacitor electrode material is growing as an energy storage material as it has various advantages. For example, it is maintenance-free, has a longer lifespan, rapid charge and discharge cycles, and can operate effectively in various environmental conditions [3]. In addition, it has > 100,000 cycles, high energy density, extensive energy storage capability, simple principles, and easy construction [4].

Based on the technique of electrical charge storage, supercapacitors are often split into two groups: electrical double-layer capacitors (EDLC) and pseudocapacitors [5]. EDLC capacitors are often utilized in low-power applications [6] using activated carbon electrodes which have a wide surface area for storing electric charge at the electrode/electrolyte interface, such as carbon fiber, carbon

aerogel, and carbon paper. The power density and stability of these capacitors are remarkable, but their specific capacitance is low[7]. In contrast, pseudocapacitors are used for high power application-swith metal oxide electrodes whose electric charge transfer is based on a reversible Faradaic process [8], including reversible adsorption, redox processes on metal oxides, and reversible electrochemical doping on conductive polymers for electrodes [9]. Pseudocapacitors can store electric charge more effectively than EDLC, but their stability is still inferior to that of EDLC. Therefore, this capacitor needs further improvement using redox-active electrode materials and increasing the specific surface area for energy storage applications in hybrid electric cars and household electric devices [10].

Supercapacitors must be designed with a high specific surface area and a narrow distribution of pore size to maximize their capacitance performance [11]. Nickel cobaltite ($NiCo_2O_4$), the electrode substance used in this study, was created by coprecipitating and calcining precursors of $NiS \cdot 5H_2O$ and $Co_2SO_4 \cdot 7H_2O$ with rGO. The spinel $NiCo_2O_4$ possesses superior electrical conductivity and redox activity than single-metal oxides like NiO and Co_3O_4. In addition, $NiCo_2O_4$ is a promising option for high-performance supercapacitors due to its high theoretical capacitance, ease of manufacture, abundant materials, low cost, and eco-friendliness.

NiO has a bandgap of 3.37 eV, a conductivity of 1.4×10^7 S/m, and a resistivity of 69.3 nΩ.m [12]. In addition, NiO is a cheap member of the transition metal oxides whose composites exhibit a mesoporous structure in the form of nanoflake crystals with a large surface area [13] as a result of the nano-dimensional electrochemical double layer mechanism with a combined faradic redox reaction [14]. This mechanism produces a maximum specific capacitance of 401 F/g at a current density of 0.5 mA/cm² [15]. Meanwhile, Co_3O_4 has an energy gap between 2.8 and 2.2 eV, a conductivity of 1.6×10^7 S/m, and a resistivity of 62.4 nm [16], with an electron mobility of 200,000 cm²/vs a specific surface area of 26,300 m²/g, an intrinsic electrochemical capacitance of 21 mF/cm², a specific capacitance of 220 F/g, a hexagonal structure with a strength of 42 N/m, and a thermal conductivity of 5,000 W/mK. Furthermore, in addition to these characteristic, the presence of other materials, such asrGO with chromophoric properties may enable Co_3O_4 to quickly absorb free electrons [17].

In order to understand how $NiCo_2O_4$ and rGO affect surface morphology, microstructure, pore size distribution, and the link between the specific surface area and the electrical properties of the supercapacitors generated, this study synthesizes and evaluates $NiCo_2O_4$/rGO nanocomposites. In addition, this study reported thermal, chemical, and electrical properties in order to explore suitability of the synthesized materual for use as supercapacitor electrodes.

2. Materials and methods

2.1. Materials

Natural graphite powder, nickel sulfide pentahydrate ($NiS \cdot 5H_2O$), cobalt sulfate hydrate ($Co_2SO_4 \cdot 7H_2O$), sulfuric acid (H_2SO_4), zinc powder (Zn), nickel nitrate ($Ni(NO_3)_2$), hydrogen peroxide (H_2O_2), aquabidest (H_2O), urea (CH_4N_2O), cobalt nitrate ($Co(NO_3)_2$), hydrochloric acid (HCl), deionized (DI) water, sodium nitrate ($NaNO_3$), citric acid ($C_6H_8O_7$), potassium permanganate ($KMnO_4$), and sodium hydroxide (NaOH) were obtained from Merck. All chemicals are of analytical grade.
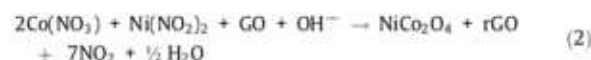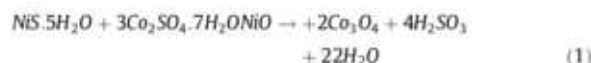
2.2. Experimental

2.2.1. Synthesis of rGO

The modified Hummers' methodwas used to synthesis rGO. As many as 2 g of graphite powder were dissolved in 98 mL of H_2SO_4 and 4 g of $NaNO_3$ while being stirred for an hour. After stirring for two hours, 8 g of $KMnO_4$ was gradually added to the mixture. Four hours were spent gently stirring the mixture in an ice container at a temperature between 0 and 20 °Cuntil it turned greenish black. At 35 °C, the mixture was agitated for 20 h until a light brown tint emerged. After beingstirred for an hour, the mixture was then washed with 200 mL of aquabidest. Once pH 7 was achieved, the mixture was centrifuged and repeatedly rinsed with 80 mL HCl and deionized water. Following that, the mixture was dried for 12 h at 110 °C to produce sheets of GO. The next phase involved adding 40 mg of GO to 40 mL of DI water, stirring it for an hour, and then ultrasonifying it for 1.5 h at 50/60 Hz. After that, GO was lowered by stirring 0.8 g of zinc powder with 10 mL of strong HCl for an hour. The mixture was added to 10 mL of concentrated HCl and stirred for an additional 30 min before being repeatedly rinsed with DI water and 5 % HCl until the pH was 7. A dry precipitate of rGOwas created by heating the precipitate from the washing process for 18 h at 160 °C in a tiny stainless steel and Teflon tube.

2.2.2. Preparation of $NiCo_2O_4$ nanoparticles

$NiS \cdot 5H_2O$ and $Co_2SO_4 \cdot 7H_2O$ were combined to form $NiCo_2O_4$ nanoparticles via coprecipitation, with a mole ratio of 1:2 (Ni^{2+}: Co^{2+}). $NiS \cdot 5H_2O$ (1.188 g) and $Co_2SO_4 \cdot 7H_2O$ (2.701 g) were dissolved in separate 20 mL of aquabidest. The solution was added dropwise to 50 mL of NaOH solution (precipitation agent) and stirred with a magnetic stirrer at 1000 rpm for one hour. The fluid was then put on a permanent magnet to speed up the deposition process. In order to get rid of any leftover salts from earlier operations, the precipitate was then rinsed seven times with DI water. After being heated in an oven at around 90 °C, the precipitate produced a black powder. The whole process is characterized by the following chemical reactions:

$$NiS \cdot 5H_2O + 3Co_2SO_4 \cdot 7H_2ONiO \rightarrow +2Co_3O_4 + 4H_2SO_3 + 22H_2O \quad (1)$$

$$2Co(NO_3) + Ni(NO_2)_2 + GO + OH^- \rightarrow NiCo_2O_4 + rGO + 7NO_2 + \frac{1}{2}H_2O \quad (2)$$

2.2.3. Fabrication of $NiCo_2O_4$/rGO nanocomposites

This nanocomposite is fabricated using rGO, $Co(NO_3)_2$, and Ni$(NO_3)_2$ as precursors. As many as 40 mg of rGO was added to 40 mL of DI water, and the mixture was stirred for an hour. Ni$(NO_3)_2$ and $Co(NO_3)_2$ powder were doped with rGO powder in various amounts (see Table 1) after two hours of agitation at 180 °C [18]. The mixture was stirred while ureaand citric acid were added. The samples were then rinsed with DI water at a pH between 6.8 and 7. The washing procedure precipitate was placed in a tiny Teflon tube within a stainless-steel tube and burnt for 18 h at 160 °C. Following a two-hour calcination at 900 °C, the resulting powder was stored. Fig. 1 shows a schematic depiction of the production process of $NiCo_2O_4$/rGOnanocomposite.

2.2.4. Characterizations of the$NiCo_2O_4$/rGO nanocomposites

$NiCo_2O_4$/rGO nanocomposites were analyzed microscopically using SEM (Scanning Electron Microscope, JEOL JSM-5310) by

Table 1

Variations in the composition of $NiCo_2O_4$/rGO nanocomposites.

Sample code	Composition of NiO:Co_2O_4:rGO (g:g:g)
S1	2:2:2
S2	2:3:2
S3	3:2:2

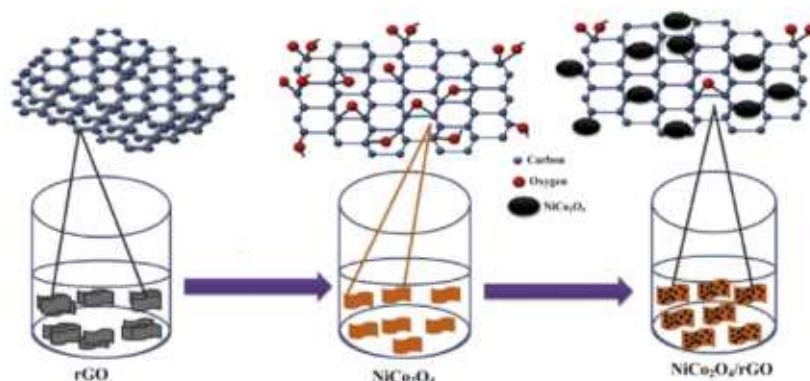**Fig. 1.** The synthesis process of NiCo$_2$O$_4$/rGO nanocomposite.

shooting electrons at 15 kV, at 50,000× magnification. Based on nitrogen adsorption–desorption measurements, the BJH (Barrett-Joyner-Halenda) and BET (Brunauer-Emmet-Teller) characterization were performed using the Sorption Analyzer NOVA 1000. Based on the N$_2$ adsorption–desorption isotherm study, this was performed at 77 K and a relative pressure of 0.05–0.30 P/P$_0$. Lastly, the electrical characteristics of graphene samples were evaluated using a CV meter, GW-Instek LCR 816, at a frequency of 1–300 kHz and an RC circuit with current propagation at four places probes.

3. Results

Analyses of the surface morphology and microstructural properties of the synthesized NiCo$_2$O$_4$/rGO, Co$_3$O$_4$/rGO, NiO/rGO, pure Co$_3$O$_4$, and pure NiO were conducted using SEM at an increasing voltage of 15 kV and a magnification of 50,000×, as presented in Fig. 2.

Based on Fig. 2a–c, the surface morphology of NiCo$_2$O$_4$/rGO nanocomposites in samples S1, S2, and S3, shows NiCo$_2$O$_4$ nanoparticles with a diamond-like hexahedron morphology on a thin transparent sheet (nanosheet) with a multilayer structure. There is folding of the rGO layer in the form of nanoflakes so that it appears thicker like large granules or clumps on the surface [19]. In addition, the presence of crystal growth such as the formation of small nano-sized needles (nanoneedles) that accumulate on the nanoplate resulting from the hydrothermal process or calcination [20].

The illustration also depicts the comparison of Co$_3$O$_4$/rGO nanocomposite (Fig. 2d) and pure Co$_3$O$_4$ (Fig. 2f) without the addition of NiO, which resemble tiny, nearly spherical lumps that are homogenous and grouped in a random manner. Meanwhile, NiO/rGO nanocomposite (Fig. 2e) and pure NiO (Fig. 2g) generated a nanoflower-like crystal structure from agglomerated NiO nanoparticles on the surface of the nickel foam substrate.

Table 2 summarizes the results of quantitative testing of the nanocomposite surface area using *Image-J Software* analysis based on the crystal structure size distribution on the material surface.

The BET test was performed to evaluate the surface area of active absorption in collecting and binding free electrons during the surface contact interaction process [21] of the NiCo$_2$O$_4$/rGO nanocomposite when it was charged to produce a type IV isothermal curve according to the IUPAC classification. Fig. 3 presents the results of BET test for S1 and S2. Meanwhile, the BJH characterization of the average pore size of NiCo$_2$O$_4$/rGO nanocomposite as a pseudocapacitive supercapacitor electrode material is presented

in Table 3. In the study of BET and BJH, we only conducted tests on S1 and S2 because the objective of this characterization was to determine whether the material synthesized was mesoporous. In addition, based on the results of the specific capacitance test, S2 exhibits the best results among the other samples, which, according to the analysis, is influenced by the abundance of Co$_3$O$_4$. Therefore, as a comparison, S1 was choosen since it had difference composition on Co$_3$O$_4$ compared to that in S2 (Fig. 4).

Electrical conductivity was analyzed since it is an important factor in storing and distributing electric charge on a polarized pseudocapacitor, which produces a potential difference between the electrodes and the solid electrolyte [22]. Fig. 5 depicts the results of electrical conductivity analysis. In addition, the average electrical conductivity and resistivity of the nanocomposites are shown in Table 4.

Specific capacitance affects the number of electrons that can be stored under pressure exerted by an electric current through a redox reaction or the ratio of the number of polarized charges per potential change [23]. The capacitance measurement was conducted utilizing a three-electrode impedance technique setup in an RC circuit. Table 5 displays the results of specific capacitance testing performed using the RC circuit-based impedance method. In addition, the following impedance equations were be used to obtain the capacitance value [24]:

$$Z = \frac{R}{1 + \left(R^2 \omega^2 C_{RC}{}^2 \right)} \tag{1}$$
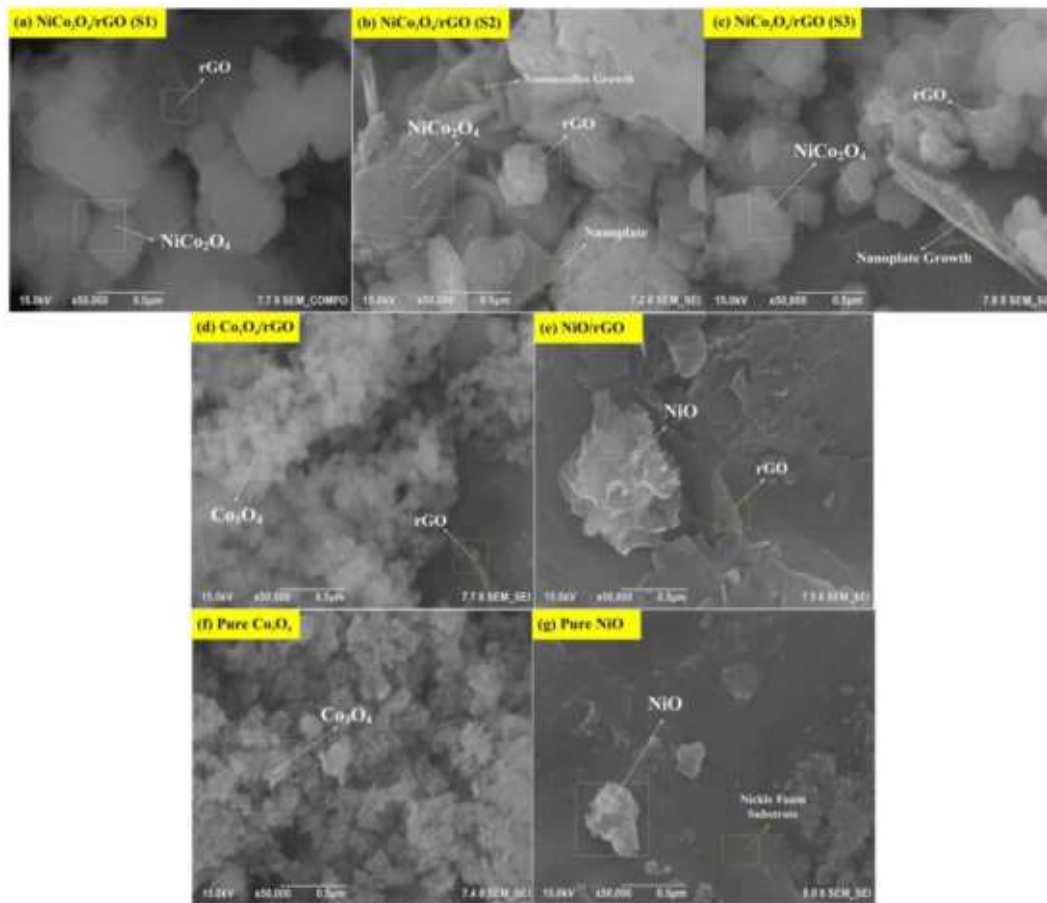
$$C = \frac{I.t}{\Delta V} \tag{2}$$

$$C_{totalpseudocapacitor} = C + C_{RLC} \tag{3}$$

$$J = \frac{I}{A} \tag{4}$$

$$E\left(\frac{Wh}{kg}\right) = \frac{Cspx\Delta V^2}{7.2} \tag{5}$$

$$P\left(\frac{W}{kg}\right) = \frac{Ex3600}{t} \tag{6}$$

where Z denotes the NiCo$_2$O$_4$/rGO nanocomposite's impedance(Ω), R denotes the RC circuit's resistance, ω is the wave propagating angular frequency (rad/s) through the sample equal to $2\pi f$, and C is the capacitance value of the sample (Farad).

Fig. 2. SEM micrograph analysis of NiCo₂O₄/rGO nanocomposites with varying NiO:Co₃O₄:rGO compositions: (a) S1 (2:2:2), (b) S2 (2:3:2), and (c) S3 (3:2:2) % wt, as well as SEM analysis of (d) Co₃O₄/rGO, (e) NiO/rGO, (f) pure Co₃O₄, and (g) pure NiO.

Table 2
Average surface area of nanocrystal structure in nanocomposite.

Types of nanocrystal form	Nanocrystal size in nanocomposites		
	Average length (μm)	Average width (μm)	Average surface area (μm^2)
Hexahedron on the structure of NiCo₂O₄	1.112	1.135	0.005
Elongated cylinders like tiny needlesinserted in nanoplate on NiCo₂O₄/rGO	0.089	0.089	3.166×10^{-4}
Nanoflower crystal structure of NiOnanoparticles and NiO/rGO	1.022	0.785	0.004
Uniform rounded lumps of Co₃O₄/rGO and Co₃O₄	0.424	0.322	0.001

According to faradaic theory, the specific surface area of the NiCo₂O₄/rGO nanocomposite is inversely proportional to its specific capacitance [25]. Numerous variables affect the specific surface area of NiCo₂O₄/rGO nanocomposites, including pore size distribution, volume, and particle diameter. By modifying the surface area of the pore structure, specific capacitance was increased. The relationship between specific capacitance and specific surface area is presented in Fig. 6.

4. Discussion

4.1. Surface morphology analysis

Fig. 2 shows the micrographs of NiCo₂O₄/rGO nanocomposites produced by coprecipitation and hydrothermally at a calcination temperature of 900 °C. They indicate that the rGO layer, which is present in the bulk, is folded and that the NiCo₂O₄ nanoparticles have a diamond-like hexahedron morphology. Crystals are formed during the hydrothermal process of calcination, as shown in the aggregation of nanoneedles on the nanoplate (Fig. 7).

4.2. Specific surface area and pore size distribution based on BET and BJH analyses

The isotherm reaction process demonstrates the unique behavior of the pores [26] in absorbing and releasing dinitrogen gas molecules (N₂)with a smaller relative pressure range (P/P₀) for samples S1 and S2 of 0.1–0.95 P/P₀ and 0.12–0.99 P/P₀, respectively. This shows that the existence of mesopores (2 nm < d < 50 nm) may be the result of detached or loose NiCo₂-O₄/rGO nanocomposite sheets on the nanoparticle stack, leading to pore gaps [19].

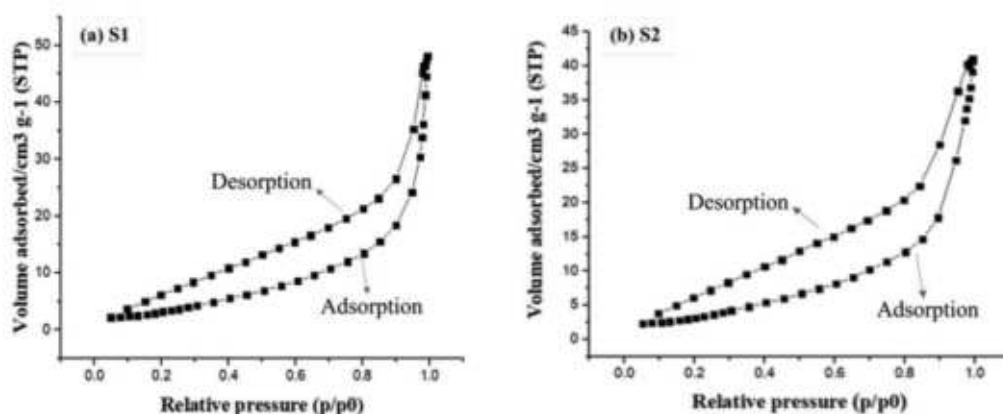**Fig. 3.** BET analysis on NiCo₂O₄/rGO nanocomposite (S1 and S2) with N₂ adsorption-desorption isotherm reaction.

Table 3
Average specific surface area, average pore radius, and total volume of NiCo₂O₄/rGO nanocomposite samples.

Sample code	Average specific surface area (m^2/g)	Average pore radius $(Å)$	Average pore volume (cm^3/g)
S1	12.90	109.77	0.07455
S2	12.75	95.34	0.06304

The NiCo₂O₄/rGO nanocomposites of S1 and S2 have average pore radii of 10.977 nm and 9.534 nm, respectively. These pore size distribution ranges, namely between 9 and 11 nm, are best in mesoporous structure since the diffusion of active species (DOS) reaction on the supercapacitor electrode materialcan increase the electrical charge storedwith these pore size distribution [27]. In addition, the pore volumes of BJH desorption for S1 and S2 are 0.00745 and 0.6304 cm³/g, respectively, and their specific surface areas are 12.90 and 12.75 m²/g, respectively. The specific surface area is crucial since it may enhance the contact interaction between the electrode and electrolyte as well as the electroactive properties by reversibly increasing the redox reaction between the electrolyte and the surface of the electroactive electrode.

4.3. Electrical properties

4.3.1. Electrical conductivity and resistivity

The results indicated that S2 has the highest electrical conductivity (6.078 S/m) and the lowest electrical resistivity (0.16 nΩ.m) compared to others. The degree of the resistivity of the compounds that make up the NiCo₂O₄/rGO nanocomposite, which is produced by the formation of crystal defects during manufacturing, affects the material's electrical conductivity. This leads awider distribution of holes on the surface of the nanocomposite particles, which prevents free electrons from being excited [28].

Based on the results (see Table 4 for S1, S2, and S3), electrical conductivity of the samples rises along with Co₃O₄ bulk. This is due to the presence of cobalt ions in cobalt oxide, which have electrical resistivities of 62.4 nΩ.m, conductivities of 1.6×10^7 S/m,
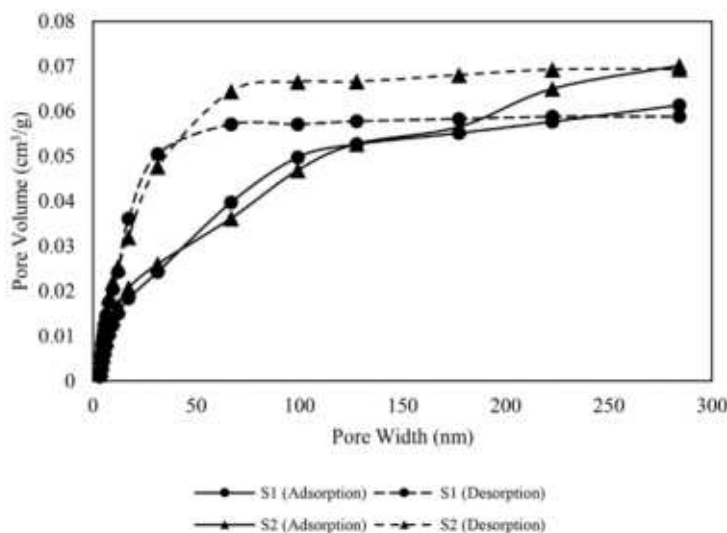

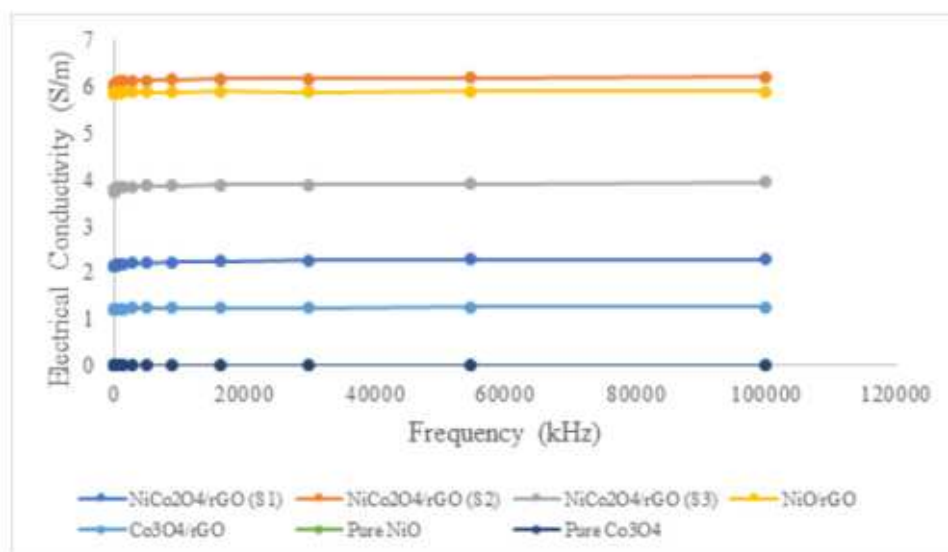**Fig. 4.** BJH pore size distribution plot of S1 and S2.

Fig. 5. Analysis of electrical conductivity from the samples in many frequencies.

Table 4
Average electrical conductivity and electrical resistivity of samples.

Sample	Average electrical conductivity (S/m)	Average electrical resistivity (nΩ.m)
S1	2.190	0.46
S2	6.078	0.16
S3	3.825	0.26
NiO/rGO	5.871	0.17
Co₃O₄/rGO	1.232	0.81
Co₃O₄	2.85×10^{-3}	350.88
NiO	1.44×10^{-3}	694.44

and bandgap energies of 2.8–2.2 eV. As a result, these conductor materials increase the electrical conductivity and electrocatalytic activity of nanocomposites during the redox reaction process [29]. The NiCo$_2$O$_4$/rGO nanocomposites causes Co$_3$O$_4$ nanoparticles to entirely dissolve, resulting in nanoparticles with perfect segmentation, low electrical resistance, high electrical conductivity, and fewer holes that might speed up the movement of free electrons.

4.3.2. Specific capacitance

The S2 sample have the highest specific capacitance, 289.93 F/g, as shown in Table 5. This suggests that increasing the bulk concentration of Co$_3$O$_4$, which carries the charge of the Co^{2+} ion, may result that increasing the specific surface area, and finally the quantity of holes to store free electrons also increase. The mobility

and oscillation of free electrons are improved when an electric field with bandgap energy is applied to the supercapacitor electrode. Free electron adsorption takes place above the bandgap of the NiCo$_2$O$_4$/rGO nanocomposite, producing electron-hole pairs that may augment the electric current with a density of 106.32 A/m^2, an energy density of 0.1573 Wh/kg, and a power density of 566.3885 W/m^3.

The specific capacitance of the NiCo$_2$O$_4$/rGO nanocomposite supercapacitor rose with an increase in current density, energy density, and power density due to the supercapacitor electrode particles' capacity to disseminate electrolyte ions in the electrode microspores [30]. It also results from the performance behavior of the NiCo$_2$O$_4$/rGO nanocomposite type supercapacitor electrodes in alkaline electrolytes during exposure to electric charge. This is influenced by an electrochemical process involving redox reactions that lead to changes in the valence electrons of Co^{3+}/Co^{4+} and M^{2+}/M^{3+} (M = Co or Ni) on the surface of the nanocomposite electrode, making the Faradaic reaction more reversible [31]. This phenomenon can be illustrated in Fig. 6. Fig. 6 depicts the reaction to generate current density when cations (H$^+$) in a solid electrolyte produce a single layer that is adsorbed on the surface of a nanocomposite electrode with a higher redox potential, such as Co^{3+}, which forms a reduced ion diffusion bridge (OH$^-$) and results in ion transfer due to the Faradaic process and oxidation of Co^{4+} elements in NiCo$_2$O$_4$/rGO.

Based on the Faradaic reaction, the chemical reaction equation that happens in NiCo$_2$O$_4$/rGO nanocomposite cells with ideal com-

Table 5
Specific capacitance, current density, energy density, and power density of samples, as determined by characterization.

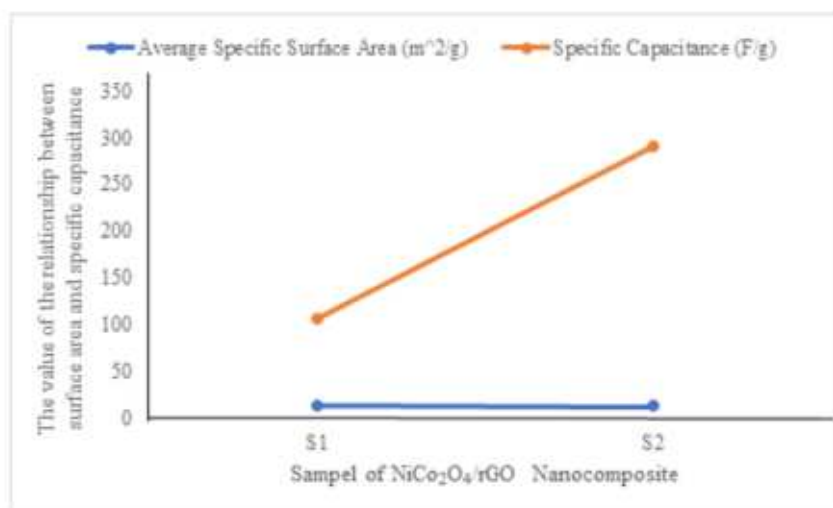| Sample	Specific capacitance (F/g)	Current density (A/m²)	Energy density (Wh/kg)	Power density (W/m³)
NiCo₂O₄/rGO (S1)	106.69	91.84	0.0760	273.5467
Ni Co₂O₄/rGO (S2)	289.93	106.32	0.1573	566.3885
Ni Co₂O₄/rGO (S3)	182.59	96.51	0.1094	393.6968
NiO/rGO	277.02	105.87	0.0726	261.4843
Co₃O₄/rGO	39.77	68.89	0.0021	7.624335
Co₃O₄	0.11	0.44	0.0018	6.4440
NiO	0.06	0.21	0.0036	12.8010

Fig. 6. Effect of specific surface area on the capacitance of $NiCo_2O_4/rGO$ nanocomposites.
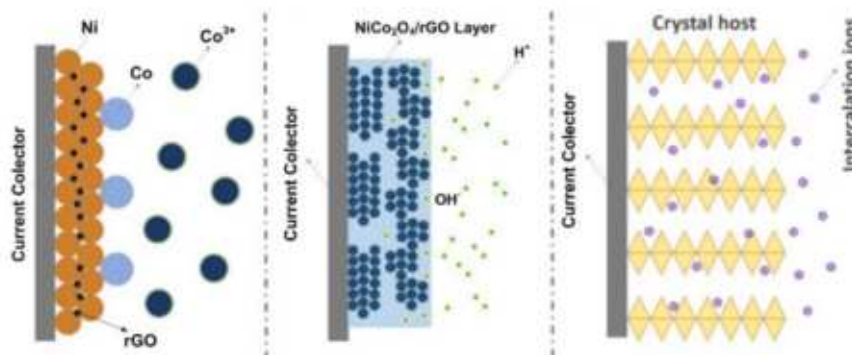

Fig. 7. Faradaic reaction process on reversible pseudocapacitance in storing electric charges.

position separated by electrolyte-soaked electron configuration can be described with the following reaction [32]:

$$CellA : NiCo_2O_4rGO|| H_2SO_4(1\ M) ||NiCo_2O_4rGO \qquad (3)$$

$$Cell\ B: NiCo_2O_4\ rGO\ ||\ KOH\ (6\ M)\ ||\ NiCo_2O_4\ rGO \qquad (4)$$

In the RC circuit containing the electrolyte solution, the redox reaction process denoted by reaction 3 and 4 is a flow of excited free electrons from the positive electrode to the negative electrode, which produces a stored electric current.

4.4. Relationship between specific surface area and specific capacitance

$NiCo_2O_4/rGO$ nanocomposites exhibit a nonlinear relationship between capacitance and surface area at all current, energy, and power densities. Due to the comparable material characteristics and pore size distribution of $NiCo_2O_4/rGO$ nanocomposite, in which the effective adsorption surface area and ion transport channel grow linearly with increasing specific surface area, the capacitance of the electric pseudocapacitor increases. Based the correlation between specific surface area and specific capacitance, the little change in specific surface area significantly affect the

specific capacitance. This is in accordance with a study by Chmiola et al. [33], which indicated that the little increase in volume pores smaller than 2 nm will significantly increase specific capacitance.

5. Conclusion

$NiCo_2O_4/rGO$ nanocomposite, which was synthesized through coprecipitation and hydrothermal methods and used as a pseudo-capacitive type supercapacitor electrode, resulted in the optimal composition for sample S2 ($NiO:Co_3O_4:rGO = 2:3:2$)compared to other samples (S1 and S3). This nanocomposite (S2) produces a hexahedron surface morphology with an average particle size of approximately 0.005 μm^2, a specific surface area of 12.75 m^2/gr, an average pore radius of 9.534 nm, and a pore volume of 0.06304 cm^3/g. In addition, S2 shows the best performance based on the analysis of electrical properties with high electrical conductivity value of 6.078 S/m, while commonly, standard supercapacitor electrode type pseudocapacitor is between 0.1 and 1 S/m. Furthermore, the electrical resistivity of S2 is 0.16 $n\Omega.m$, which is the lowest (best) among others (S1 and S3). The capacitance value of S2 is the highest, which is 289.93 F/g, while generally, the standard pseudocapacitor type for $NiCo_2O_4$ is 120 F/g.

CRediT authorship contribution statement

Andriono Manalu: Conceptualization, Methodology, Investigation, Writing – original draft. **Kerista Tarigan:** Validation, Supervision, Writing – review & editing. **Syahrul Humaidi:** Supervision, Funding acquisition, Visualization. **Masno Ginting:** Data curation, Resources. **Istas Pratomo Manalu:** Formal analysis, Investigation. **Ikhwanuddin:** Investigation, Project administration.

Declaration of Competing Interest

The authors declare that they have no known competing financial interests or personal relationships that could have appeared to influence the work reported in this paper.

Acknowledgments

References

[1] X. Zhang, L. Hou, A. Ciesielski, P. Samorì, 2D Materials Beyond Graphene for High-Performance Energy Storage Applications, Adv. Energy Mater. 6 (23) (2016) 1600671, https://doi.org/10.1002/aenm.201600671.

[2] J. Wang et al., 'Thermal Charging' Phenomenon in Electrical Double Layer Capacitors, Nano Lett. 15 (9) (2015) 5784–5790, https://doi.org/10.1021/acs.nanolett.5b01761.

[3] C. Liu, Q. Li, K. Wang, State-of-charge estimation and remaining useful life prediction of supercapacitors, Renew. Sustain. Energy Rev. 150 (2021) https://doi.org/10.1016/j.rser.2021.111408 111408.

[4] T. Huang et al., Tri-high designed graphene electrodes for long cycle-life supercapacitors with high mass loading, Energy Storage Mater. 17 (2019) 349–355, https://doi.org/10.1016/j.ensm.2018.07.001.

[5] S. Karthikeyan, B. Narenthiran, A. Sivanantham, L.D. Bhatlu, T. Maridurai, Supercapacitor: Evolution and review, Mater. Today: Proc. 46 (2021) 3984–3988, https://doi.org/10.1016/j.matpr.2021.02.526.

[6] M. Zhou, A. Gallegos, K. Liu, S. Dai, J. Wu, Insights from machine learning of carbon electrodes for electric double layer capacitors, Carbon N. Y. 157 (2020) 147–152, https://doi.org/10.1016/j.carbon.2019.08.090.

[7] S. Faraji, F.N. Ani, The development supercapacitor from activated carbon by electroless plating–A review, Renew. Sustain. Energy Rev. 42 (2015) 823–834, https://doi.org/10.1016/j.rser.2014.10.068.

[8] S. Najib, E. Erdem, Current progress achieved in novel materials for supercapacitor electrodes: mini review, Nanoscale Adv. 1 (8) (2019) 2817–2827, https://doi.org/10.1039/C9NA00345B.

[9] A.A. Mohd Abdah, N.H.N. Azman, S. Kulandaivalu, Y. Sulaiman, Review of the use of transition-metal-oxide and conducting polymer-based fibres for high-performance supercapacitors, Mater. Des. 186 (2020), https://doi.org/10.1016/j.matdes.2019.108199 108199.

[10] J.-S.-M. Lee, M.E. Briggs, C.-C. Hu, A.I. Cooper, Controlling electric double-layer capacitance and pseudocapacitance in heteroatom-doped carbons derived from hypercrosslinked microporous polymers, Nano Energy 46 (Apr. 2018) 277–289, https://doi.org/10.1016/j.nanoen.2018.01.042.

[11] J. Chang et al., Activated porous carbon prepared from paulownia flower for high performance supercapacitor electrodes, Electrochim. Acta 157 (2015) 290–298, https://doi.org/10.1016/j.electacta.2014.12.169.

[12] S.M. Kabbur, S.D. Waghmare, U.R. Ghodake, S.S. Suryavanshi, Synthesis, morphology and electrical properties of Co2+ substituted NiCuZn ferrites for MLCI applications, 2018, p. 130002. 10.1063/1.5029072.

[13] P.E. Saranya, S. Selladurai, Mesoporous 3D network Ce-doped NiO nanoflakes as high performance electrodes for supercapacitor applications, New J. Chem. 43 (19) (2019) 7441–7456, https://doi.org/10.1039/C9NJ00097F.

[14] K.M. Thulasi, S.T. Manikkoth, A. Paravannoor, S. Palantavida, M. Bhagiyalakshmi, B.K. Vijayan, Ceria deposited titania nanotubes for high performance supercapacitors, J. Phys. Chem. Solids 135 (2019), https://doi.org/10.1016/j.jpcs.2019.109111 109111.

[15] S. Ghosh, W.D. Yong, E.M. Jin, S.R. Polaki, S.M. Jeong, H. Jun, Mesoporous carbon nanofiber engineered for improved supercapacitor performance, Korean J. Chem. Eng. 36 (2) (2019) 312–320, https://doi.org/10.1007/s11814-0199-1.

[16] D. Zhang, C. Jiang, P. Li, Y. Sun, Layer-by-Layer Self-assembly of Co₃O₄ Nanorod-Decorated MoS₂ Nanosheet-Based Nanocomposite toward High-Performance Ammonia Detection, ACS Appl. Mater. Interfaces 9 (7) (2017) 6462–6471, https://doi.org/10.1021/acsami.6b15669.

[17] M. Hareesha, B. Yogesha, L.L. Naik, D. Saravanabavan, Development on graphene based polymer composite materials and their applications—A recent review, 2021, p. 030016. 10.1063/5.0036854.

[18] A. Manalu, et al., Synthesis, Microstructure and Electrical Properties of NiCo2O4/rGO composites as Pseudocapacitive Electrode for Supercapacitors, Int. J. Electrochem. Sci. ArticleID: 22036, Mar. 2022, 10.20964/2022.03.11.

[19] Y. Li et al., NiCo2O4 particles with diamond-shaped hexahedron structure for high-performance supercapacitors, Appl. Surf. Sci. 436 (2018) 242–251, https://doi.org/10.1016/j.apsusc.2017.12.025.

[20] P.S. Shewale, K.-S. Yun, NiCo2O4/RGO Hybrid Nanostructures on Surface-Modified Ni Core for Flexible Wire-Shaped Supercapacitor, Nanomaterials 11 (4) (2021) 852, https://doi.org/10.3390/nano11040852.

[21] Z. Yang et al., Multiform Sulfur Adsorption Centers and Copper-Terminated Active Sites of Nano-CuS for Efficient Elemental Mercury Capture from Coal Combustion Flue Gas, Langmuir 34 (30) (2018) 8739–8749, https://doi.org/10.1021/acs.langmuir.8b01181.

[22] R.S. Kate, S.A. Khalate, R.J. Deokate, Overview of nanostructured metal oxides and pure nickel oxide (NiO) electrodes for supercapacitors: A review, J. Alloys Compd. 734 (2018) 89–111, https://doi.org/10.1016/j.jallcom.2017.10.262.

[23] M. Mirzaeian, Q. Abbas, D. Gibson, M. Mazur, Effect of nitrogen doping on the electrochemical performance of resorcinol-formaldehyde based carbon aerogels as electrode material for supercapacitor applications, Energy 173 (2019) 809–819, https://doi.org/10.1016/j.energy.2019.02.108.

[24] W. Choi, H.-C. Shin, J. M. Kim, J.-Y. Choi, W.-S. Yoon, Modeling and Applications of Electrochemical Impedance Spectroscopy (EIS) for Lithium-ion Batteries, J. Electrochem. Sci. Technol. 11(1) (2020) 1–13. 10.33961/jecst.2019.00528.

[25] K. Song, R. Yang, X. Chen, X. Wang, G. Chen, N. Zhao, The structures of CoFe2O4/PEDOT electrodes effect on the stability and specific capacity for electrochemical energy storage, Appl. Surf. Sci. 542 (2021), https://doi.org/10.1016/j.apsusc.2020.148670 148670.

[26] H.M. Jennings, A. Kumar, G. Sant, Quantitative discrimination of the nano-pore-structure of cement paste during drying: New insights from water sorption isotherm, Cem. Concr. Res. 76 (2015) 27–36, https://doi.org/10.1016/j.cemconres.2015.05.006.

[27] X. Zhou et al., Improved Oxygen Reduction Reaction Performance of Co Confined in Ordered N-Doped Porous Carbon Derived from ZIF-67@PILs, Ind. Eng. Chem. Res. 56 (39) (2017) 11100–11110, https://doi.org/10.1021/acs.iecr.7b03417.

[28] Y. Zhang et al., Influence of chemical disorder on energy dissipation and defect evolution in concentrated solid solution alloys, Nat. Commun. 6 (1) (2015) 8736, https://doi.org/10.1038/ncomms9736.

[29] T.E.P. Alves, H.V.S. Pessoni, A. Franco Jr., The effect of Y³⁺ substitution on the structural, optical band-gap, and magnetic properties of cobalt ferrite nanoparticles, PCCP 19 (25) (2017) 16395–16405, https://doi.org/10.1039/C7CP02167D.

[30] L. Qin et al., High area energy density of all-solid-state supercapacitor based on double-network hydrogel with high content of graphene/PANI fiber, Chem. Eng. J. 430 (2022), https://doi.org/10.1016/j.cej.2021.133045 133045.

[31] A. Lv, S. Lu, W. Xu, Z. Wang, Y. Shen, G. Liu, One-pot synthesis of NiCo2O4/rGO/NF hybrid electrode materials realizing ultrahigh capacitance and rapid charge/discharge at large current density, Appl. Surf. Sci. 511 (2020), https://doi.org/10.1016/j.apsusc.2020.145538 145538.

[32] P. Salarizadeh, M.B. Askari, M. Seifi, S.M. Rozati, S.S. Eisazadeh, Pristine NiCo2O4 nanorods loaded rGO electrode as a remarkable electrode material for asymmetric supercapacitors, Mater. Sci. Semicond. Process. 114 (2020), https://doi.org/10.1016/j.mssp.2020.105078 105078.

[33] J. Chmiola, G. Yushin, R. Dash, Y. Gogotsi, Effect of pore size and surface area of carbide derived carbons on specific capacitance, J. Power Sources 158 (1) (Jul. 2006) 765–772, https://doi.org/10.1016/j.jpowsour.2005.09.008.

Effect of surface area on electrical properties of NiCo2O4-reduced graphene oxide nanocomposites for supercapacitor electrodes applications

6   Internet Source   <1%

7   ysjskxygc.xml-journal.net
    Internet Source   <1%

8   Debasree Burman, Ruma Ghosh, Sumita Santra, Samit Kumar Ray, Prasanta Kumar Guha. " Role of vacancy sites and UV-ozone treatment on few layered MoS nanoflakes for toxic gas detection ", Nanotechnology, 2017
    Publication   <1%

9   Submitted to Sabanci Universitesi
    Student Paper   <1%

10 Zhong, Shan, Chuanxing Zhan, and Dapeng Cao. "Zeolitic imidazolate framework-derived nitrogen-doped porous carbons as high performance supercapacitor electrode materials", Carbon, 2015.
    Publication   <1%

11 www.repository.cam.ac.uk
    Internet Source   <1%

12 Jing Fan Yang, Pingwei Liu, Volodymyr B. Koman, Albert Tianxiang Liu, Michael S. Strano. "Synthetic Cells: Colloidal-sized state machines", Elsevier BV, 2019
    Publication   <1%

13 Sobia Dilpazir, Pengju Ren, Rongji Liu, Menglei Yuan et al. "Efficient Tetra-Functional Electrocatalyst with Synergetic Effect of Different Active Sites for Multi-Model Energy Conversion and Storage", ACS Applied Materials & Interfaces, 2020
Publication

<1%

14 journals.pan.pl
Internet Source

<1%

15 Submitted to Jeju National University
Student Paper

<1%

16 Submitted to Universiti Sains Islam Malaysia
Student Paper

<1%

17 Submitted to Myongji University Graduate School
Student Paper

<1%

18 eprints.ums.edu.my
Internet Source

<1%

19 www.eaiib.agh.edu.pl
Internet Source

<1%

20 Submitted to Indira Gandhi Delhi Technical University for Women
Student Paper

<1%

21 keep.lib.asu.edu
Internet Source

<1%

22 researcher.life
Internet Source
<1%

23 theses.insa-lyon.fr
Internet Source
<1%

24 ar.booksc.eu
Internet Source
<1%

25 opus.lib.uts.edu.au
Internet Source
<1%

26 Li Zhao, Li-Zhen Fan, Meng-Qi Zhou, Hui Guan, Suyan Qiao, Markus Antonietti, Maria-Magdalena Titirici. "Nitrogen-Containing Hydrothermal Carbons with Superior Performance in Supercapacitors", Advanced Materials, 2010
Publication
<1%

27 polen.itu.edu.tr:8443
Internet Source
<1%

28 scholars.cityu.edu.hk
Internet Source
<1%

29 Abduelwhab. B. Alwany, G. M. Youssef, O. M. Samir, Mohammed A. Algradee et al. "Annealing temperature effects on the size and band gap of ZnS quantum dots fabricated by co-precipitation technique without capping agent", Scientific Reports, 2023
<1%

30	**pure-test.amc.nl** Internet Source	<1%
31	**www.deswater.com** Internet Source	<1%
32	**Submitted to University of New Haven** Student Paper	<1%
33	**www.journaltocs.ac.uk** Internet Source	<1%
34	**repositori.usu.ac.id:8080** Internet Source	<1%
35	**www.ukaazpublications.com** Internet Source	<1%
36	Jie Liang, Haitao Zhao, Luchao Yue, Guangyin Fan, Tingshuai Li, Siyu Lu, Guang Chen, Shuyan Gao, AbdullahM. Asiri, Xuping Sun. "Recent advances in electrospun nanofibers for supercapacitors", Journal of Materials Chemistry A, 2020 Publication	<1%
37	Jun Yan, Qian Wang, Tong Wei, Zhuangjun Fan. "Recent Advances in Design and Fabrication of Electrochemical Supercapacitors with High Energy Densities", Advanced Energy Materials, 2014 Publication	<1%

38 Submitted to Universidade Estadual de Campinas
Student Paper
<1 %

39 Submitted to University of Leeds
Student Paper
<1 %

40 Submitted to University of Rijeka
Student Paper
<1 %

41 pure.sruc.ac.uk
Internet Source
<1 %

42 Submitted to University of Cincinnati
Student Paper
<1 %

43 Submitted to University of Utah
Student Paper
<1 %

44 Submitted to 于 2013-04-17 提交至 Univerza v Ljubljani
Student Paper
<1 %

45 ceramics.onlinelibrary.wiley.com
Internet Source
<1 %

46 dacemirror.sci-hub.st
Internet Source
<1 %

47 researchportal.be
Internet Source
<1 %

48 Submitted to University of Ulster
Student Paper
<1 %

49 joiv.org
Internet Source
<1%

50 livrepository.liverpool.ac.uk
Internet Source
<1%

51 www.tandfonline.com
Internet Source
<1%

52 Yunita Sari Pane, Yetty Machrina, Nurfida Khairina Arrasyid, Mutiara Indah Sari. "The effect of chewing-betel habits on blood glucose levels in the Karo ethnic community, Karo district", F1000Research, 2022
Publication
<1%

53 api.openalex.org
Internet Source
<1%

54 khazna.ku.ac.ae
Internet Source
<1%

55 www.asra.com
Internet Source
<1%

56 www.mediasphera.ru
Internet Source
<1%

57 Stefan Bade. "DEVELOPMENT OF A NEW REACTOR FOR COMBINED COMMINUTION AND CHEMICAL REACTION", Chemical Engineering Communications, 1/1/1996
Publication
<1%

58   Syahrul Humaidi, Rini Mutiara Putri Damanik, Ikhwanuddin, Winelda Mahfud Zaidan Haris. "Study on hydrochar nanostructure from durian skin waste reinforced by gum arabic as an organic ink", AIP Publishing, 2020
Publication   <1 %

59   core-cms.prod.aop.cambridge.org
Internet Source   <1 %

60   espace.library.uq.edu.au
Internet Source   <1 %

61   jme.biam.ac.cn
Internet Source   <1 %

62   ksascholar.dri.sa
Internet Source   <1 %

63   Laurent Karim Béland, Chenyang Lu, Yuri N. Osetskiy, German D. Samolyuk, Alfredo Caro, Lumin Wang, Roger E. Stoller. "Features of primary damage by high energy displacement cascades in concentrated Ni-based alloys", Journal of Applied Physics, 2016
Publication   <1 %

64   Obreja, V.V.N.. "On the performance of supercapacitors with electrodes based on carbon nanotubes and carbon activated material-A review", Physica E: Low-   <1 %

dimensional Systems and Nanostructures, 200805
Publication

65   Siauciunas, R.. "Influence of tobermorite texture and specific surface area on CO"2 chemisorption", Colloids and Surfaces A: Physicochemical and Engineering Aspects, 20040906
Publication

<1 %

66   Yutong Han, Da Huang, Yujie Ma, Guili He, Jun Hu, Jing Zhang, Nantao Hu, Yanjie Su, Zhihua Zhou, Yafei Zhang, Zhi Yang. " Design of Hetero-Nanostructures on MoS Nanosheets To Boost NO Room-Temperature Sensing ", ACS Applied Materials & Interfaces, 2018
Publication

<1 %

Exclude quotes	Off	Exclude matches	Off
Exclude bibliography	Off		